

# Polarization Transfer in Wide-Angle Compton Scattering and Single-Pion Photoproduction from the Proton

C. Fanelli,<sup>1</sup> E. Cisbani,<sup>2</sup> D. J. Hamilton,<sup>3</sup> G. Salmé,<sup>1</sup> B. Wojtsekhowski,<sup>4,\*</sup> A. Ahmidouch,<sup>5</sup>  
 J. R. M. Annand,<sup>3</sup> H. Baghdasaryan,<sup>6</sup> J. Beaufait,<sup>4</sup> P. Bosted,<sup>4</sup> E. J. Brash,<sup>7,4</sup> C. Butuceanu,<sup>8</sup>  
 P. Carter,<sup>7</sup> E. Christy,<sup>9</sup> E. Chudakov,<sup>4</sup> S. Danagoulian,<sup>5</sup> D. Day,<sup>6</sup> P. Degtyarenko,<sup>4</sup> R. Ent,<sup>4</sup> H. Fenker,<sup>4</sup>  
 M. Fowler,<sup>4</sup> E. Frlez,<sup>6</sup> D. Gaskell,<sup>4</sup> R. Gilman,<sup>4,10</sup> T. Horn,<sup>4</sup> G. M. Huber,<sup>8</sup> C. W. de Jager,<sup>4,6</sup>  
 E. Jensen,<sup>7</sup> M. K. Jones,<sup>4</sup> A. Kelleher,<sup>11</sup> C. Keppel,<sup>9</sup> M. Khandaker,<sup>12</sup> M. Kohl,<sup>9</sup> G. Kumbartzki,<sup>10</sup>  
 S. Lassiter,<sup>4</sup> Y. Li,<sup>9</sup> R. Lindgren,<sup>6</sup> H. Lovelace,<sup>12</sup> W. Luo,<sup>13</sup> D. Mack,<sup>4</sup> V. Mamyan,<sup>6</sup> D. J. Margaziotis,<sup>14</sup>  
 P. Markowitz,<sup>15</sup> J. Maxwell,<sup>6</sup> G. Mbianda,<sup>16</sup> D. Meekins,<sup>4</sup> M. Meziane,<sup>11</sup> J. Miller,<sup>17</sup> A. Mkrtchyan,<sup>18</sup>  
 H. Mkrtchyan,<sup>18</sup> J. Mulholland,<sup>6</sup> V. Nelyubin,<sup>19</sup> L. Pentchev,<sup>11</sup> C. F. Perdrisat,<sup>11</sup> E. Piassetzky,<sup>20</sup>  
 Y. Prok,<sup>7</sup> A. J. R. Puckett,<sup>21</sup> V. Punjabi,<sup>12</sup> M. Shabestari,<sup>6</sup> A. Shahinyan,<sup>18</sup> K. Slifer,<sup>6</sup>  
 G. Smith,<sup>4</sup> P. Solvignon,<sup>22</sup> R. Subedi,<sup>6</sup> F. R. Wesselmann,<sup>12</sup> S. Wood,<sup>4</sup> Z. Ye,<sup>9</sup> and X. Zheng<sup>6</sup>

<sup>1</sup>*Dipartimento di Fisica, Università La Sapienza, Rome, Italy and INFN, Sezione di Roma, 00185, Rome, Italy*

<sup>2</sup>*INFN, Sezione di Roma, gruppo Sanità and Istituto Superiore di Sanità, 00161 Rome, Italy*

<sup>3</sup>*University of Glasgow, Glasgow G12 8QQ, Scotland, U.K.*

<sup>4</sup>*Thomas Jefferson National Accelerator Facility, Newport News, VA 23606*

<sup>5</sup>*North Carolina A&T State University, Greensboro, NC 27411*

<sup>6</sup>*University of Virginia, Charlottesville, VA 22904*

<sup>7</sup>*Christopher Newport University, Newport News, VA 23606*

<sup>8</sup>*University of Regina, Regina, SK S4S 0A2, Canada*

<sup>9</sup>*Hampton University, Hampton, VA 23668*

<sup>10</sup>*Rutgers, The State University of New Jersey, Piscataway, NJ 08855*

<sup>11</sup>*College of William and Mary, Williamsburg, VA 23187*

<sup>12</sup>*Norfolk State University, Norfolk, VA 23504*

<sup>13</sup>*Lanzhou University, Lanzhou 730000, Gansu, Peoples Republic of China*

<sup>14</sup>*California State University Los Angeles, Los Angeles, CA 90032*

<sup>15</sup>*Florida International University, Miami, FL 33199*

<sup>16</sup>*University of Witwatersrand, Johannesburg, South Africa*

<sup>17</sup>*University of Maryland, College Park, MD 20742*

<sup>18</sup>*Yerevan Physics Institute, Yerevan 375036, Armenia*

<sup>19</sup>*St. Petersburg Nuclear Physics Institute, Gatchina, 188350, Russia*

<sup>20</sup>*University of Tel Aviv, Tel Aviv, Israel*

<sup>21</sup>*Massachusetts Institute of Technology, Cambridge, MA 02139*

<sup>22</sup>*Argonne National Laboratory, Argonne, IL, 60439*

(Dated: April 18, 2022)

Wide-angle exclusive Compton scattering and single-pion photoproduction from the proton have been investigated via measurement of the polarization transfer from a circularly polarized photon beam to the recoil proton. The WACS polarization transfer was analyzed at an incident photon energy of 3.7 GeV at a proton scattering angle of  $\theta_{\gamma}^{\text{cm}} = 70^\circ$ . The longitudinal transfer  $K_{\text{LL}}$ , measured to be  $0.645 \pm 0.059 \pm 0.048$ , where the first error is statistical and the second is systematic, has the same sign as predicted for the reaction mechanism in which the photon interacts with a single quark carrying the spin of the proton. However, the observed value is  $\sim 3$  times larger than predicted by the GPD-based calculations, which indicates a significant unknown contribution to the scattering amplitude.

PACS numbers: 13.60.Fz, 14.20.Dh

Understanding the structure of hadrons in terms of QCD is one of the fundamental goals of modern nuclear physics. The formalism of Generalized Parton Distributions (GPD), developed about 20 years ago, for the first time linked hadron structure information accessible through inclusive reactions such as Deep Inelastic Scattering (DIS) to information from exclusive reactions. These GPDs, while not di-

rectly measurable in experiments, provide a unified description of key electromagnetic reactions on the nucleon [1]. Whereas DIS allows investigation of the longitudinal structure of the nucleon, exclusive reactions such as elastic electron and photon scattering access its transverse structure. Taken together they allow determination of a complete image of the nucleon and its complex substructure [2].

Wide-angle Compton Scattering (WACS) from the nucleon with large values of  $s$ ,  $-t$ , and  $-u$  compared with  $\Lambda_{\text{QCD}}^2$  is a hard exclusive process which provides access to information about nucleon structure that is complementary to high  $Q^2$  elastic form factors and Deeply Virtual Compton Scattering. The common feature of these reactions is a large energy scale, leading to factorization of the scattering amplitude into a hard perturbative kernel and a factor described by soft non-perturbative wave functions.

Various theoretical approaches have been applied to WACS in the hard-scattering regime, and these can be distinguished by the number of active quarks participating in the hard subprocess, or equivalently, by the mechanism for sharing the transferred momentum among the constituents. Two extreme pictures have been proposed. In the perturbative QCD (pQCD) approach, three active quarks share the transferred momentum by the exchange of two hard gluons [3, 4]. In the handbag approach, which has in recent years become a staple in the interpretation of data from hard exclusive reactions, only one quark, whose wave function has sufficient high-momentum components for the quark to absorb and re-emit the photon [5–7], is assumed to be active. In any given kinematic regime both mechanisms will contribute, in principle, to the cross section. It is generally believed that at sufficiently high energies the pQCD mechanism dominates. However, in the currently accessible experimental domain of  $s$  and  $t$ , the nature of the reaction mechanism is not fully understood.

Three other theoretical advances based on leading-quark dominance in WACS have been proposed in recent years. The constituent quark model with a handbag diagram has proven successful in describing the WACS process [8], as have calculations performed in a generalized Vector Meson Dominance (VMD) framework [9]. More recently, the soft-collinear effective theory (SCET) was developed for elastic electron-proton scattering at high momentum transfer [10]. The QCD factorization approach formulated in the framework of SCET allows for the development of a description of the soft-spectator scattering contribution to the overall amplitude. The two-photon exchange contributions to elastic electron-proton scattering were shown to factorize by the introduction of a single, universal SCET form-factor which defines the dominant soft-spectator amplitudes. As it is argued in Refs. [10], the same form factor also naturally arises in WACS and the most promising route for understanding this soft spectator contribution in hard exclusive reactions at JLab energies is the study of WACS.

One of the main predictions of the pQCD mechanism for WACS is the constituent scaling rule [11], whereby  $d\sigma/dt$  scales as  $s^{-6}$  at fixed  $\theta_\gamma^{\text{cm}}$ . The pioneering experiment at Cornell [12] was approximately consistent with constituent scaling, albeit with modest statistical precision. However, the high-precision data from JLab gave a scaling power of  $s^{-7.5\pm 0.2}$  [13]. The calculations from both the GPD-based handbag approach and the SCET framework have reproduced the JLab cross section data very well. Crucially, the extracted values of the SCET form factor do not show any significant dependence on the value of  $s$  as required by factorization.

The longitudinal and sideways polarization transfer observables,  $K_{\text{LL}}$  and  $K_{\text{LS}}$ , respectively, are defined by:

$$K_{\text{LL}} \equiv \frac{d\sigma(\rightarrow\rightarrow) - d\sigma(\leftarrow\leftarrow)}{d\sigma(\rightarrow\rightarrow) + d\sigma(\leftarrow\leftarrow)},$$

$$K_{\text{LS}} \equiv \frac{d\sigma(\rightarrow\uparrow) - d\sigma(\leftarrow\uparrow)}{d\sigma(\rightarrow\uparrow) + d\sigma(\leftarrow\uparrow)},$$

where the first arrow refers to the incident photon helicity and the second to the recoil proton longitudinal ( $\rightarrow$ ) or sideways ( $\uparrow$ ) polarization. The polarization transfer observables were previously measured at JLab for Compton scattering at a different kinematics of  $s = 6.9$  and  $t = -4.1$  GeV<sup>2</sup> in experiment E99-114 [14] whose concept is mainly repeated here at different kinematic. It was found that the longitudinal component of the polarization transfer at this kinematic point is large and positive, in agreement with the handbag GPD and SCET predictions, and in unambiguous disagreement with the pQCD predictions.

The measurement reported in this letter (the JLab experiment E07-002) was carried out in Hall C at Jefferson Lab, with the purpose of providing values of  $K_{\text{LL}}$  and  $K_{\text{LS}}$  when all the Mandelstam variables are larger than  $\Lambda_{\text{QCD}}^2$ . The layout of the experiment is shown schematically in Fig. 1. A longitudinally polarized, 100% duty-factor electron beam with current up to 40  $\mu\text{A}$  and energy of 4.11 GeV was incident on a copper radiator of 1.3 mm thickness placed on the beam line. The mixed beam of electrons and bremsstrahlung photons was incident on a 15-cm liquid H<sub>2</sub> target, located just downstream of the radiator, with a photon flux of up to 10<sup>13</sup> equivalent quanta/s. For incident photons at an average weighted energy of 3.7 GeV, the scattered photon were detected at a scattering angle of 25.7° in the BigCal calorimeter, which is composed of 1744 lead-glass bars subtending a solid angle of 34 msr with an angular resolution of 1.8 mrad and relative energy resolution of 12%. The associated recoil proton was

detected in the Hall C High Momentum Spectrometer (HMS) at the corresponding central angle of  $40^\circ$  and central momentum of 1.85 GeV. The proton was detected within a solid angle of 5 msr and momentum acceptance of  $\pm 9\%$ . The trigger was formed from a coincidence between a signal from scintillator counters in the HMS and a signal above a 500 MeV threshold in the calorimeter. A magnet between the target and the calorimeter, as shown in Fig. 1, with  $\int \vec{B} \times d\vec{l} = 1.2$  Tm deflected the elastically scattered electrons vertically by  $\sim 50$  cm relative to undeflected WACS photons. Events with a radiative photon kinematically indistinguishable from WACS constitute an irreducible background.

Data have been collected with the radiator present and removed, and with different field settings of the deflection magnet. About 7.4 C of beam charge was accumulated for WACS production runs. The electron beam longitudinal polarization was found to be  $75.0 \pm 1.1\%$  using a Møller polarimeter. During data taking, the beam polarization was flipped at a 30 Hz rate. The bremsstrahlung photon has 99% of the initial electron polarization over the energy range of current analysis.

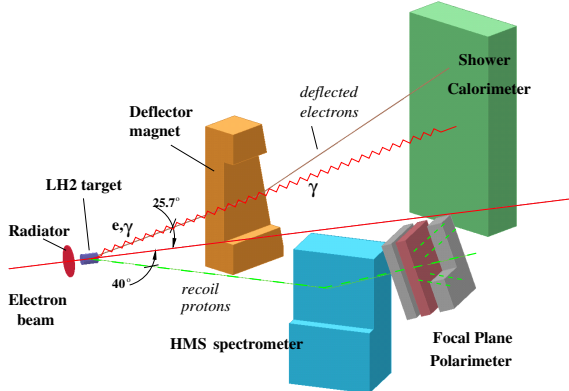


FIG. 1: Schematic layout of the E07-002 experiment.

Potential WACS events are selected based on the kinematic correlation between the scattered photon and the recoil proton. The known optical properties of the HMS are used to reconstruct the momentum, direction, and reaction vertex of the recoil proton, from which the reconstructed incident photon (electron) energy (assuming a  $\gamma p$  and  $ep$  final state),  $E_{\text{inc}}$  was determined. The  $\delta x$  and  $\delta y$ , the difference in  $x$  and  $y$  coordinates between the expected and measured locations of the scattered photon at the entrance of the calorimeter were calculated. The distributions of events in the  $(\delta x : \delta y)$  and  $(E_{\text{inc}} : \delta y)$  planes are shown in Fig. 2 and 3, respectively.

The WACS events  $p(\gamma, \gamma'p)$ , which are concentrated in the peak at  $\delta x, \delta y \sim 0$  cm, lie on top

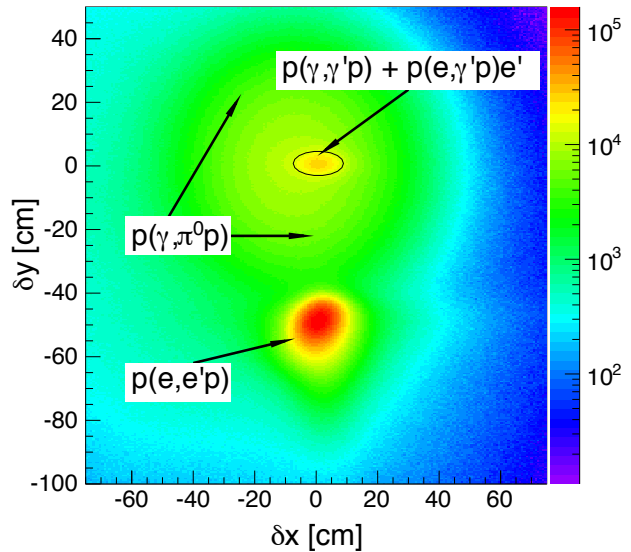


FIG. 2: 2D distribution of events in  $(\delta x : \delta y)$ . The WACS events  $p(\gamma, \gamma'p)$  and the irreducible Bethe-Heitler background  $p(e, \gamma'p)e'$  form the peak at  $\delta x, \delta y \sim 0$  cm, which is selected by an elliptical cut  $(\delta x/8)^2 + (\delta y/4)^2 < 1$ . This region also contains the photo-pion events  $p(\gamma, \pi^0 p)$  underlying continuum. The  $ep$  elastic events are centered at  $\delta x \sim 0$ ,  $\delta y \sim 50$  cm.

of a continuum background mainly related to the  $p(\gamma, \pi^0 p)$  reaction, for which one of the photons is detected from the subsequent decay  $\pi^0 \rightarrow \gamma\gamma$ . An additional background is due to electrons and radiative photons from elastic  $ep$  scattering.

The recoil proton polarization was measured by the focal plane polarimeter (FPP) located in the HMS. The FPP determines the two polarization components normal to the momentum of the proton by measuring the azimuthal asymmetries in the angular distribution after secondary scattering of the proton from an analyzer for positive and negative electron beam-helicity states. Two 60 cm (53 g/cm<sup>2</sup>) thick blocks of CH<sub>2</sub> analyzers were used in the experiment. Two drift chambers at the focal plane, and a pair of large-acceptance drift chambers placed after each analyzer, tracked the protons before, between, and after the analyzer blocks, effectively producing two independent polarimeters with a combined figure-of-merit (a product of efficiency and analyzing power in square) of  $7 \times 10^{-3}$ .

For each analyzer, the angular distribution of the scattered protons is given by

$$N(\vartheta, \varphi) = N_0(\vartheta) \left\{ 1 + [A_y(\vartheta) P_t^{\text{FPP}} + \alpha] \sin \varphi - [A_y(\vartheta) P_n^{\text{FPP}} + \beta] \cos \varphi \right\},$$

where  $N_0$  is the number of protons which scatter in the polarimeter,  $\vartheta$  and  $\varphi$  are the polar and azimuthal scattering angles,  $P_n^{\text{FPP}}$  or  $P_t^{\text{FPP}}$  are the helicity-dependent components of the proton polarization at

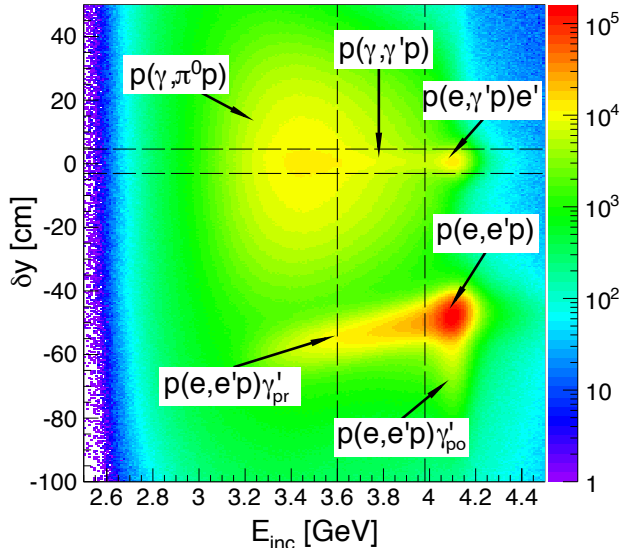


FIG. 3: 2D distribution of events in  $(E_{\text{inc}}: \delta y)$ . WACS  $p(\gamma, \gamma' p)$  events are concentrated around  $\delta y \sim 0$  cm, selected through an elliptical cut in  $(\delta x : \delta y)$ , and reconstructed  $E_{\text{inc}} \in [3.60, 3.98]$  GeV. The  $p(e, \gamma' p) e'$  events, with a high energy post-scattering radiative photon, are at  $E_{\text{inc}} = 4.1$  GeV. Photo-pion  $p(\gamma, \pi^0 p)$  events are mainly located at  $\delta y \sim 0$  cm and  $E_{\text{inc}} < 3.6$  GeV. At  $\delta y = -50$  cm and  $E_{\text{inc}} = 4.1$  GeV, elastic  $p(e, e' p)$  events form a peak, with a vertical tail in  $\delta y$  of  $p(e, e' p) \gamma'_{po}$  with a post-scattering radiative photon, and an oblique tail of  $p(e, e' p) \gamma'_{pr}$  with a pre-scattering radiative photon.

the FPP,  $A_y$  is the FPP analyzing power, and  $\alpha$  and  $\beta$  are helicity-independent terms including instrumental asymmetries. Such a distribution was measured for the two states of the electron beam-helicity. The difference between these two distributions,  $N^+/N_0^+ - N^-/N_0^-$ , cancels the instrumental asymmetries to first order and gives access to the helicity-dependent transferred polarization. Performing a Fourier analysis of the beam-helicity difference of  $N(\vartheta, \varphi)$  allows extraction of the products of the proton polarization components and  $A_y$  shown in Fig. 4.

Determination of  $A_y(\vartheta)$  for each of the analyzers was performed by measuring the longitudinal polarization of the recoil proton from  $\bar{e}p$  elastic scattering at approximately the same proton momentum. This analysis also yields the ratio of the proton elastic form factors, which was found to be  $\mu_p G_E^p / G_M^p = 0.744 \pm 0.031$  at  $Q^2 = 2.25$  GeV<sup>2</sup>, in excellent agreement with a fit to known measurements [15].

Polarization components at the FPP were related to their counterparts at the target by calculating the proton spin precession in the HMS. This was done by using a COSY model [16] of the HMS optics to obtain a spin transport matrix for each proton track. The elements of this matrix are characterized by

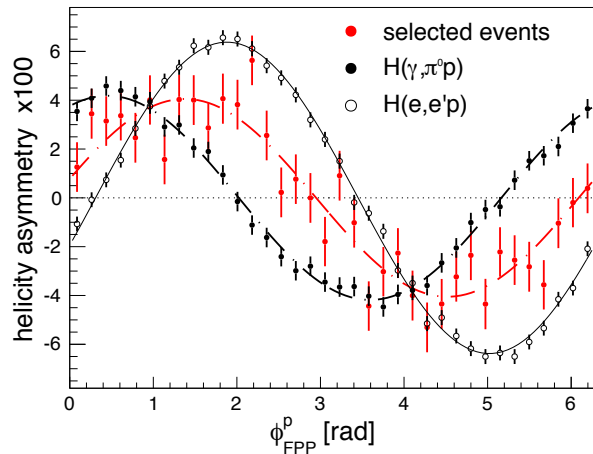


FIG. 4: Azimuthal variation of the difference between beam-helicity correlated proton rates. The selected events (filled red circles), are identified with an elliptical cut, see Fig. 2. Also shown are the corresponding asymmetries for the main background events: the elastic  $ep$  (open white circles), and photo-pion (filled black circles).

the average spin precession angle, which is approximately  $100^\circ$ . The proton spin vector was then transformed to the proton rest frame, with the longitudinal axis pointing in the direction of the recoil proton in the center-of-mass frame [6]. In that frame, the longitudinal and sideways components of the proton polarization normalized to the photon polarization are just the spin transfer parameters  $K_{LL}$  and  $K_{LS}$ , respectively.

The WACS events are selected from a small elliptical region at the origin of the  $(\delta x : \delta y)$  plane, as shown in Fig. 2. For each spin component, the following deconvolution procedure has been used to extract the final WACS recoil polarization  $P_{\text{WACS}}$ :

$$\begin{aligned} P_{\text{peak}} &= [P_{\text{ellipse}} - (1 - f_1)P_{\text{pion}}] / f_1, \\ P_{\text{WACS}} &= [P_{\text{peak}} - (1 - f_2)P_{ep\gamma}] / f_2, \end{aligned}$$

where  $P_{\text{ellipse}}$ ,  $P_{\text{peak}}$ ,  $P_{\text{pion}}$  and  $P_{ep\gamma}$  are the polarizations related to (i) all of the events within the  $(\delta x : \delta y)$  ellipse shown in Fig. 2, (ii) only the events in the peak above the continuum background, (iii) the pion photoproduction background events, and (iv) the Bethe-Heitler background events. The fractions for the ratio of event types are defined as  $f_1 = N_{\text{peak}} / N_{\text{ellipse}}$  and  $f_2 = N_{\text{WACS}} / N_{\text{peak}}$ , respectively. The dominant background polarization, by itself an important physics results,  $P_{\text{pion}}$ , was measured by selecting events from regions of the  $(\delta x : \delta y)$  plane in Fig. 2 that contain neither WACS nor  $ep$  ( $ep\gamma$ ) events, corresponding to  $\delta y > 10$  cm and  $-35 < \delta y < -10$  cm. It was found that within the statistical precision of the measurements,  $P_{\text{pion}}$  was constant over broad regions of that plane. The polar-

ization of the  $ep\gamma$  background  $P_{ep\gamma}$  was determined by selecting events in the deflected  $ep$  elastic peak region. It was determined that within the statistical precision, the polarization  $P_{ep}$  was consistent with  $P_{ep\gamma}$ . The results for the longitudinal and sideways components are  $P_{ep\gamma}^{LL} = 0.4513 \pm 0.0054$  and  $P_{ep\gamma}^{LS} = -0.1837 \pm 0.0054$ . Systematic uncertainties arising from the methods used to determine the background polarization observables have been studied and included in the final results. The final source of background which needs to be taken into account arises as a result of the presence of accidental random events in the final sample ( $<4\%$  of the events).

Results obtained with the two polarimeters were statistically consistent and were combined to form a weighted mean. With the WACS region selected to obtain the best statistical accuracy on  $P_{WACS}$  and fits performed on the respective distributions, we find  $f_1 = 0.405 \pm 0.004$ . The determination of the fraction  $f_2$  is a little more involved and requires analysis of calibration data taken without the copper radiator. By doing so, we measure the quantity  $n_{ep\gamma} = N_{ep\gamma}/N_{ep}$  after having imposed an optimized cut on the incident energy to remove pre-vertex interactions, which can then be used to determine the fraction  $f_2 = 1 - N_{ep\gamma}/N_{peak} = 1 - n_{ep\gamma} \times N_{ep}/N_{peak}$  for the production data. Following this method, we find  $f_2 = 0.67 \pm 0.03$ . As a consistency check, this fraction was determined using a second analysis method which involved reconstructing the incident energy spectrum for  $ep\gamma$  events through a convolution of the theoretical bremsstrahlung spectrum from the radiator with the real spectrum of calibration events (without the radiator) for a scattered photon detected at  $\delta y \sim 0$  cm. A third method consists of extracting the fraction from the difference between the value of the cross section measured in this experiment, which includes the irreducible  $ep\gamma$  background, and the value of the WACS cross section obtained from the parametrization of the E99-114 results [13]. The results obtained for  $f_2$  using these three methods were found to be consistent with each other.

TABLE I: The WACS polarization transfer results. The values of the Mandelstam variables are  $s = 7.8$  (0.3) and  $t = -2.1$  (0.1)  $\text{GeV}^2$ , which define  $\theta_\gamma^{\text{cm}} = 70$  ( $2^\circ$ ) (The values in parentheses are the acceptance ranges.). For the WACS polarization the first uncertainty is statistical and the second is systematic.

	$P_{\text{ellipse}}$	$P_{\text{peak}}$	$P_{\text{WACS}} = K_{LL} (K_{LS})$
LL	$0.180 \pm 0.015$	$0.565 \pm 0.038$	$0.645 \pm 0.059 \pm 0.048$
LS	$-0.233 \pm 0.015$	$-0.142 \pm 0.038$	$-0.089 \pm 0.059 \pm 0.040$

TABLE II: A comparison between E99-114 [14] and current results. In E99-114,  $s = 6.9 \text{ GeV}^2$  and  $\theta_\gamma^{\text{cm}} = 120^\circ$ , whereas in this experiment  $s = 7.8 \text{ GeV}^2$  and  $\theta_\gamma^{\text{cm}} = 70^\circ$ . The longitudinal and sideways observables for the single-pion photo-production and WACS are shown.

	$P_{\text{pion}}^{\text{E99-114}}$	$P_{\text{pion}}^{\text{this exp.}}$	$P_{\text{WACS}}^{\text{E99-114}}$
LL	$0.532 \pm 0.006$	$-0.082 \pm 0.007$	$0.678 \pm 0.083 \pm 0.04$
LS	$0.480 \pm 0.006$	$-0.296 \pm 0.007$	$0.114 \pm 0.078 \pm 0.04$

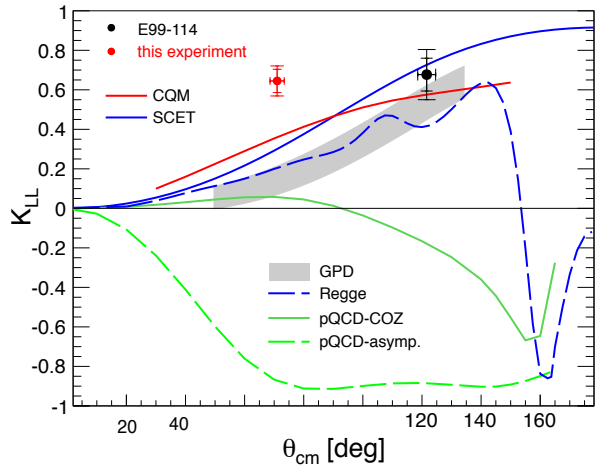


FIG. 5: The experimental result for  $K_{LL}$ . Also shown is the E99-114 value [14]. The calculations in different approaches: the asymptotic and COZ both from the pQCD [4, 18], the extended Regge model [9], the GPD [7] shown as a grey band of uncertainty due to finite mass corrections [19], the CQM [8], the SCET [10].

The extracted polarization transfer observables for different event samples are given in Table I. A comparison between the E99-114 [14] and the present polarization measurement results for WACS and a single-pion photo-production is given in Tables I and II. The large change of  $K_{LL}$  in pion production between the two data sets indicates a complicated non-asymptotic reaction mechanism. These results are in good agreement with previous measurements [17]. The final result for WACS  $K_{LL}$  is shown in Fig. 5 along with the predictions of the relevant calculations. In agreement with what was found in the previous JLab experiment [14], the  $K_{LL}$  result is inconsistent with predictions based on the pQCD theory [4] and hence suggests that even at this experiment values of  $s, -t, -u = 7.8, 2.1, 4.0 \text{ GeV}^2$  we are still far from the asymptotic regime for the WACS process. Figure 5 shows predictions for the two extreme choices of distribution amplitudes (DAs), namely the asymptotic and COZ [18] cases, with all other DAs providing intermediate values.

In conclusion, the polarization transfer observables  $K_{LL}$  and  $K_{LS}$  have been measured for proton Compton scattering at a new kinematic point at  $s=7.8 \text{ GeV}^2$  and  $\theta_\gamma^{\text{cm}} = 70^\circ$ . The final results are  $K_{LL} = 0.645 \pm 0.059 \pm 0.048$  and  $K_{LS} = -0.089 \pm 0.059 \pm 0.040$ , where the first uncertainty is statistical and the second is systematic. The  $K_{LS}$  result is in agreement within the experimental uncertainties with calculations for both the leading-quark and the pQCD approaches [4, 7, 8, 10] and hence suggests that there is no strong evidence for proton helicity-flip in this reaction. The value obtained for  $K_{LL}$  is, quite unexpectedly, larger than all the available theoretical predictions. Such a  $K_{LL}$  could be caused by non-collinear effects in exclusive reactions at currently accessible energies and parton correlations in the nucleon. In this respect, the  $K_{LL}$  increase may be related to significant roles observed in elastic electron-nucleon scattering of both quark orbital angular momentum and a  $u-d$  diquark correlation [20, 21].

We thank the Jefferson Lab Hall C technical staff for their outstanding support. This work was supported in part by the INFN gruppo Sanità, the National Science Foundation, the UK Science and Technology Facilities Council, and the DOE under contract DE-AC05-84ER40150 Modification No. M175, under which the Southeastern Universities Research Association (SURA) operates the Thomas Jefferson National Accelerator Facility.

---

\* Corresponding author: bogdanw@jlab.org

[1] D. Müller *et al.*, *Fortschr. Phys.* **42**, 101 (1994); X.D. Ji, *Phys. Rev. Lett.* **78**, 610 (1997); A.V. Radyushkin, *Phys. Lett. B* **380**, 417 (1996).  
 [2] A.V. Belitsky and A.V. Radyushkin, *Phys. Rep.* **418** 1 (2005).  
 [3] G.R. Farrar and H. Zhang, *Phys. Rev. Lett.* **65**, 1721

(1990), *Phys. Rev. D* **42**, 3348 (1990).  
 [4] A.S. Kronfeld and B. Nizic, *Phys. Rev. D* **44**, 3445 (1991); M. Vanderhaeghen, P.A.M. Guichon and J. Van de Wiele, *Nucl. Phys. A* **622**, 144c (1997); T. Brooks and L. Dixon, *Phys. Rev. D* **62** 114021 (2000).  
 [5] A.V. Radyushkin, *Phys. Rev. D* **58**, 114008 (1998).  
 [6] M. Diehl, T. Feldmann, R. Jakob, P. Kroll, *Eur. Phys. J. C* **8**, 409 (1999).  
 [7] H.W. Huang, P. Kroll, T. Morii, *Eur. Phys. J. C* **23**, 301 (2002), *Erratum ibid.*, **C 31**, 279 (2003).  
 [8] G.A. Miller, *Phys. Rev. C* **69**, 052201(R) (2004).  
 [9] F. Cano and J.M. Laget, *Phys. Lett. B* **551**, 317 (2003).  
 [10] N. Kivel and M. Vanderhaeghen, *J. High Energy Phys.* **4**, 1 (2013); *Nucl. Phys. B* **883**, 224 (2014); arXiv:1504.00991.  
 [11] S.J. Brodsky and G. Farrar, *Phys. Rev. Lett.* **31**, 1153 (1973); V.A. Matveev, R.M. Muradyan, and A.V. Tavkheldize, *Lett. Nuovo Cimento* **7**, 719 (1973).  
 [12] M.A. Shupe *et al.*, *Phys. Rev. D* **19**, 1921 (1979).  
 [13] A. Danagoulian *et al.*, *Phys. Rev. Lett.* **98**, 152001 (2007).  
 [14] D.J. Hamilton *et al.*, *Phys. Rev. Lett.* **94**, 242001 (2005).  
 [15] A.J.R. Puckett *et al.*, *Phys. Rev. C* **85**, 045203 (2012).  
 [16] K. Makino and M. Berz, *Nucl. Instr. Meth. A* **427**, 338 (1999).  
 [17] K. Wijesooriya *et al.*, *Phys. Rev. C* **66**, 034614 (2002); W. Luo *et al.*, *Phys. Rev. Lett.* **108**, 222004 (2012).  
 [18] V.L. Chernyak, A.A. Oglobin, and A.R. Zhitnitsky, *Z. Phys. C* **42**, 569 (1989).  
 [19] M. Diehl, Th. Feldmann, H.W. Huang, and P. Kroll, *Phys. Rev. D* **67**, 037502 (2003).  
 [20] M. Jones *et al.*, *Phys. Rev. Lett.* **84**, 1398 (2000); O. Gayou *et al.*, *Phys. Rev. Lett.* **88**, 092301 (2002); G.A. Miller, *Phys. Rev. C* **66**, 032201(R) (2002).  
 [21] G. Cates *et al.*, *Phys. Rev. Lett.* **106**, 252003 (2011); C.D. Roberts *et al.*, *Eur. Phys. J. ST* **140**, 53 (2007); I.C. Cloët *et al.*, *Few-Body Systems* **46**, 1(2009).